This is a preprint, the final version is subject to change, of the American Mineralogist (MSA)
Cite as Authors (Year) Title. American Mineralogist, in press.
(DOI will not work until issue is live.) DOI: http://dx.doi.org/10.2138/am-2017-5864

Igneous or Metamorphic? Hornblende Phenocrysts as Greenschist Facies Reaction Cells in the Half Dome Granodiorite, California

Revision 2

STEPHEN C. CHALLENER[1] AND ALLEN F. GLAZNER

Department of Geological Sciences, University of North Carolina, Chapel Hill, NC 27599-3315, U.S.A.

ABSTRACT

The Half Dome Granodiorite, Yosemite National Park, California, is recognized in the field by euhedral, fresh-looking, black hornblende phenocrysts up to 2 cm in length. This variety of granodiorite typifies intermediate-age hornblende-phyric units of Cretaceous nested plutonic suites in the Sierra Nevada batholith. Although only inclusions of feldspar are evident in hand sample, the phenocrysts are riddled with up to 50% inclusions of every major mineral found in the host granodiorite plus metamorphic minerals formed during cooling. Amphibole compositions within single phenocrysts vary from actinolite with less than 1 wt% Al_2O_3 to magnesiohornblende with over 8 wt%. Elemental zoning within the amphibole is highly irregular on the μm scale, showing patches and polygonal zones with dramatically different compositions separated by sharp to gradual transitions. The chemical compositions of entire phenocrysts are equivalent to hornblende plus a small proportion of biotite, suggesting that the non-biotite inclusions are the result of metamorphism of the phenocrysts. Backscattered electron imaging shows evidence of brecciation which may have been the result of volume changes as hornblende

[1] Present address
Department of Marine, Earth, and Atmospheric Sciences
NC State University
Raleigh, North Carolina, USA 27695

was converted to actinolite. Pressure calculations using the Al-in-hornblende barometer show unreasonably wide variations on the μm scale that cannot have been produced by temperature or pressure variations during crystallization. These hornblende phenocrysts would thus be unsuitable for geobarometry, and caution must be used to avoid similarly zoned phenocrysts in the application of the Al-in-hornblende geobarometer.

INTRODUCTION

What are phenocrysts, and what do they signify? In both plutonic and volcanic rocks, crystals that are much larger than their surrounding matrix are generally interpreted as having grown early in a magma's crystallization history (e.g., Harker and Marr 1891; Crosby 1900; Kelley and Branson 1947; Vernon 1986; Straub and Martin-Del Pozzo 2001). In volcanic rocks this interpretation is generally unambiguous, because volcanic rocks are cooled rapidly from the magmatic state and thus freeze in magmatic texture, and experiments can duplicate observed volcanic phase assemblages and textures (e.g., Lofgren 1980; Johnson and Rutherford 1989).

However, textural interpretation is more challenging in plutonic rocks because such rocks are not quenched but rather cool over periods of up to millions of years (Coleman et al. 2004), allowing ample time for chemical and textural modification. For example, Davis et al. (2012) found that some plutons emplaced at shallow levels in the Sierra Nevada of California took up to 10 m.y. to cool below 300 °C. This means that they could have spent millions of years at temperatures corresponding to the greenschist and amphibolite facies, and that temperature may have oscillated during cooling owing to emplacement of new increments of magma. In addition, phase equilibria studies show that some common phenocrystic phases, such as K-feldspar megacrysts that reach sizes over 10 cm (Gilbert 1906; Bateman 1961; Booth 1968), cannot be

This is a preprint, the final version is subject to change, of the American Mineralogist (MSA)
Cite as Authors (Year) Title. American Mineralogist, in press.
(DOI will not work until issue is live.) DOI: http://dx.doi.org/10.2138/am-2017-5864

early crystallization products (Johnson and Glazner 2010; Glazner and Johnson 2013). Thus, interpretation of phenocrysts in plutonic rocks can be ambiguous.

Hornblende and biotite commonly form large (cm-scale), euhedral phenocrysts in granodiorites. In contrast to K-feldspar, both experimental studies and the petrography of volcanic rocks show that they can be near-liquidus phases in intermediate magmas (Piwinskii 1968; Naney and Swanson 1980; Devine et al. 1998). For such phenocrysts, unlike K-feldspar megacrysts, large size and euhedral habit are not surprising, and their textural origin has remained unquestioned.

The Half Dome Granodiorite is the middle unit of the nested Late Cretaceous Tuolumne Intrusive Suite of Yosemite National Park, California (Fig. 1; Bateman and Chappell 1979; Bateman, 1992). As with most plutons, this unit was defined and mapped on the basis of its texture—primarily the presence of large, euhedral hornblende phenocrysts that can reach up to 2 cm in length (Fig. 2; Dodge et al. 1968; Coleman et al. 2005). Hornblende is a particularly important phase in plutonic rocks because it offers one of the only barometers available for igneous rocks—the Al-in-hornblende geobarometer (Hammarstrom and Zen 1986; Anderson and Smith 1995). In a plutonic rock emplaced at a given depth and then cooled, core-to-rim Al zoning should be a function of slow isobaric cooling, with Al content primarily reflecting the pressure of emplacement.

Hornblende phenocrysts in the Half Dome Granodiorite commonly weather out intact (Fig. 2), and thus they can be sectioned through their centers in known orientations. In this study we examined a number of such phenocrysts. Far from displaying a simple story of isobaric cooling, these phenocrysts contain copious inclusions of other minerals and have extreme, irregular, fine-scale zoning in Al.

METHODS

Euhedral hornblende phenocrysts ranging from 1 to 2 cm in maximum dimension were collected from grus developed on the Half Dome Granodiorite exposed in glacial pavement west of Tenaya Lake. On glacial pavements throughout this area, weathering releases intact hornblende and biotite phenocrysts (Fig. 2A). Intact phenocrysts also weather out on surfaces that were not glaciated, such as the top of Half Dome.

Five large, intact, solid, fresh-appearing hornblende phenocrysts were mounted in epoxy, sawn, and polished. Because of their large size, euhedral form and easy removal from matrix, the phenocrysts can be precisely oriented relative to their crystal axes. Four were cut perpendicular to the **c**-axis and one perpendicular to the **a**-axis, all through their centers. The polished phenocrysts were examined in a Tescan VEGA 5136 scanning electron microscope at the University of North Carolina using backscattered electron (BSE) imagery, and X-ray maps were generated using a Sirius Si-drift detector and 4pi Revolution software.

Element maps were exported as image files and run through a Gaussian low-pass filter with a kernel size of 9x9 to reduce noise. These images were then imported into ENVI GIS software for mapping. Regions of interest were placed on representative mineral inclusions, which were readily identified by their X-ray spectra. A supervised classification was then performed using the minimum distance method to identify and map all mineral inclusions in the images (Fig. 2C; Supplemental Fig. 1).

Chemical analyses and high-resolution images were collected on a JEOL JXA-8530F field-emission Hyperprobe at Fayetteville State University with an accelerating voltage of 15 kV, calibrated against Astimex standards. Typical beam size was 1 µm. Pressures were calculated from these compositions using the Al-in-hornblende geobarometer as implemented by Anderson et al. (2008).

RESULTS

The hornblende phenocrysts host copious inclusions of every other mineral species in the rock (Figs. 2,3,4). These include abundant biotite largely altered to chlorite, magnetite, plagioclase, K-feldspar, apatite, and titanite, with minor amounts of quartz, albite, epidote, clinozoisite, zircon, and muscovite. Inclusions average 45 area % of the five mapped phenocrysts, with biotite+chlorite comprising 17 area % (Fig. 3).

There is little obvious pattern to the distribution of inclusions. Some biotite crystals are aligned with (001) parallel to crystal faces of the enclosing phenocryst, but most are not. In phenocryst 3 (Fig. 2), biotite+chlorite crystals seem to form a concentric zone about ½ diameter out from the center, whereas in phenocryst 5 (Fig. 5) there is a concentric zone of complex feldspar crystals at about the same distance from center.

BSE and microprobe analyses show that the amphibole zones of the phenocrysts are strongly zoned on a fine scale (Figs. 4,5,6), and that this zoning is not systematic. Spot analyses range from magnesiohornblende to actinolite (Fig. 6; Table 1). Despite the presence of non-hornblende amphibole compositions we will continue to refer to the amphiboles collectively as hornblende. Compositional parameters are tightly correlated above 2 wt% Al_2O_3; for example, MgO shows a strong negative correlation (Fig. 6), and FeO a strong positive correlation, with Al_2O_3. Because FeO and Al_2O_3 exhibit strong positive correlation, BSE image brightness correlates directly with Al_2O_3, which varies by 5 wt% over a length scale of tens of μm (Fig. 7) in an irregular, patchy manner. A number of low-MgO, high-FeO points lie off this trend at low

Al_2O_3, trending toward ferroactinolite (Fig. 6). These latter points are almost exclusively located immediately adjacent to zones of chloritized biotite.

The amphibole areas show a number of small-scale modes of zoning. These vary from sharply defined polygons to blurred zones with rounded edges to zig-zag patterns. Some blurring is likely due to slanted interfaces that are sharper than they appear. Some zones are uniform in composition, whereas others show internal compositional gradients (Fig. 7). In places the zoning pattern suggests healed fractures in which high-Al materials fill gaps in low-Al actinolite; this is particularly evident where compositional boundaries are zig-zag (Fig. 7A,B,C).

There is no indication of concentric compositional zoning as is commonly seen in igneous phenocrysts. For example, cm-scale hornblende phenocrysts in Montserrat andesite display concentric oscillatory zones that likely reflect mixing events (Rutherford and Devine 2003; Humphreys et al. 2009). Such oscillatory zoning is common in hornblende in many volcanic systems (e.g., Bachmann and Dungan 2002; Sato et al. 2005; Humphreys et al. 2006). However, the phenocrysts in this study only show patchy, irregular zoning. Although compositional variability within the hornblende is extreme, there is no apparent pattern of compositional variation with distance from a phenocryst's center (Fig. 6), even along a smooth core-to-rim track.

Five complete 2-cm-long, euhedral phenocrysts, and three composites of 2-3 euhedral phenocrysts, were analyzed for major elements by X-ray fluorescence (Table 1). These phenocrysts were freed of crystals clinging to their faces, although feldspar inclusions intersecting the crystal surfaces were common. These analyses, which represent the bulk volumes enclosed by the phenocryst boundaries, lie at the high-Al_2O_3 end of the spot analyses for most elements but are significantly higher in K_2O and lower in CaO and Na_2O, showing values intermediate between high-Al hornblende and biotite analyses from within the phenocrysts (Fig. 8). P_2O_5 concentrations averaging 0.6 wt% indicate about 1.5 wt% apatite in the phenocrysts, assuming that the *P* content of the hornblende is on the order of 500 ppm or less (Bachmann et al. 2005).

DISCUSSION

The maps and imagery show that these hornblende phenocrysts contradict common assumptions about the nature of phenocrysts. Not only are they heavily included, but many of the included minerals are late-magmatic or subsolidus products in plutonic systems, such as K-feldspar. Because K-feldspar crystallizes late in magma of this composition (Johnson and Glazner 2010) the phenocrysts could not have grown around these inclusions if hornblende crystallized in a largely liquid magma. The extreme and irregular elemental zoning within the hornblende also cannot reflect compositional variations occurring during a single crystallization event. Furthermore, the huge range in amphibole composition within single phenocrysts makes the Al-in-hornblende geobarometer difficult to apply.

Hornblende phenocrysts from the Half Dome Granodiorite do not show the features predicted for unmodified crystals that grew in a largely liquid magma. Extreme textural modification is suggested by the alteration of biotite into chlorite, as well as the wide array of greenschist-grade mineral inclusions, including chlorite, albite and epidote, and the broad range of amphibole compositions. Slow cooling of incrementally emplaced plutonic rocks may have left them at pressure (*P*) and temperature (*T*) conditions within the amphibolite and greenschist facies for extended periods of time (Davis et al. 2012; Glazner and Johnson 2013). The compositions of whole phenocrysts are also essentially those of the high-Al end of measured hornblende compositions plus approximately 5-30 wt% biotite (Fig. 8), with the exception of Fe which is slightly higher in the bulk analyses. This suggests suggesting that the included minerals developed from normal hornblende phenocrysts that contained inclusions of biotite and possibly magnetite, without any change in bulk composition. Using our measured high-Al hornblende (*Hbl*) and actinolite (*Act*) compositions with quartz (Qtz), end-member albite (*Ab*), K-feldspar (*Or*), magnetite (*Mt*), and zoisite (*Zo*), one such balanced reaction is

$$Hbl + 0.07Qtz = 0.71Act + 0.11Ab + 0.05Or + 0.09Mt + 0.10Zo$$

This reaction also provides an explanation for why quartz, which is abundant in the host rock, is rarely found in the inclusion population.

Conversion of hornblende to actinolite can induce a decrease in volume, causing microcracks within the crystal (Okamoto and Toriumi 2005). This may provide an explanation for the brecciated compositional zones in Figures 4 and 7. In most cases crack filling appears to consist of higher-Al (and thus higher-T) amphibole than the host material. However, the patterns are too complicated to reflect a single brecciation event. This suggests that repeated episodes of brecciation may have been caused by cyclical changes in temperature; cooling would drive the reaction to the right, causing cracking due to loss in volume, followed by heating that would heal the cracks with higher-Al amphibole. Such a scenario implies that temperatures oscillated across the greenschist-amphibolite facies boundary, consistent with the multi-million-year intervals between hornblende and biotite Ar ages (Davis et al. 2012). Highly angular zones may thus represent more recent episodes, while rounded or blurred zones show earlier episodes which have undergone diffusive relaxation.

Thus, despite their euhedral shape, the texture and mineralogy of the phenocrysts have been completely overwritten. Replacement of hornblende by actinolite and patchy zoning between actinolite and hornblende are typical of amphibole porphyroblasts (Gibbons and Horak

1984, Klein 1969, Grapes 1974) rather than phenocrysts, suggesting that the phenocrysts record a significant metamorphic history. The wide range of large, well-formed secondary minerals developed from the Half Dome phenocrysts is, however, a unique feature not typical of purely metamorphic or igneous amphiboles. This may be another anomalous texture caused by variations in temperature. Rapid crystal coarsening by thermal cycling is a well-documented phenomenon, and has been suggested as an important coarsening mechanism in petrology (Johnson and Glazner 2010). It may be that initially small or diffuse reaction products within the phenocrysts were condensed into larger crystals by this mechanism. It is also possible that the phenocrysts themselves were coarsened by this mechanism; however, given the common occurrence of volcanic hornblende phenocrysts it is possible that their initial size was simply the result of early growth.

Whatever their genesis, the strong and aconcentric Al zoning and development of secondary minerals observed in the phenocrysts indicate that pressure information is masked and difficult to extract from spot analyses of hornblende phenocrysts in the Half Dome Granodiorite. The actinolite end of the trend is clearly meaningless, but which Al content records the pressure is subject to interpretation. Hammarstrom and Zen (1986) discarded crystals which were altered to actinolite riddled with opaques, and Anderson and Smith (1995) omitted “Al-poor subsolidus amphiboles.” However, in our samples, where there is a continuum in Al from hornblende down to clearly metamorphic actinolite, there is no clear break in Al below which analyses can be confidently discarded (Gray et al. 2008)

The best estimate of the predominant hornblende composition lies where the biotite-addition lines intersect the main amphibole trend (Fig. 8). This intersection occurs at ~7 wt% Al_2O_3 for most elements. This value can be used with the Al-in-hornblende barometer (Anderson and Smith 1995) to calculate P. Figure 9 shows calculated *P* as a function of *T* for this Al content. Also shown are (1) hornblende-plagioclase thermobarometry on Half Dome Granodiorite (Gray et al. 2008) and (2) *P-T* estimates from aplite dikes, using the method outlined in Putnam et al. (2015), which assumes that aplite whole-rock compositions are equivalent to liquids separated from a quartz-, feldspar-, and zircon-bearing crystalline mush, and that the magma was water-saturated with a water activity of unity. Aplite analyses from the Tenaya Lake region are from Glazner et al. (2008). These estimates scatter near the water-saturated granite solidus at low pressure (130±70 MPa) using the Zr calibration of Watson and Harrison (1983); temperatures calculated using the Boehnke et al. (2013) calibration are systematically ~60 °C cooler and well below the solidus. Solution of the hornblende thermobarometer is *T*-dependent, and isobaric cooling should cause a rimward decrease in Al, so it is difficult to determine an appropriate T, although it should be higher than those recorded by the near-solidus aplite dikes. At T > 730 °C (the maximum *T* recorded by the aplite dikes), *P* estimates for the hornblende are consistent with those of the aplites.

Gray et al. (2008) noted that Half Dome hornblende crystals range from magnesiohornblende to actinolite but did not explain how analyses were screened for thermobarometry. Presumably they used the higher-Al analyses. Our new data, Gray et al.'s results, and the aplite thermobarometry indicate cooling at *P* ~ 150 MPa, and thus a depth of around 6±2 km assuming a crustal density of 2700 kg/m^3. Ague and Brimhall (1988) made a regional study of pressures calculated using the hornblende barometer. They reported no analyses of hornblende from the Half Dome Granodiorite, but Tenaya Lake lies in a regional low-*P* zone (~100-200 MPa), consistent with our data.

We have observed abundant biotite in the cores of hornblende in granodiorites and tonalites in the Tuolumne Intrusive Suite, and they are not uncommon throughout the Sierra Nevada (e.g., Frost and Mahood 1987). However, the pervasive occurrence of biotite cores in hornblende went largely unremarked in previous studies of the Tuolumne Intrusive Suite (e.g., Bateman and Chappell 1979; Gray et al. 2008). If this relationship reflects order of crystallization then it contradicts the common assumption that biotite follows hornblende. For example, Abbott (1981) noted that "In a series of comagmatic intrusions related by differentiation, the biotite almost always appears later than the hornblende, in agreement with the reaction series of Bowen (1928). Certainly the sequence hornblende, biotite + hornblende, biotite in differentiated granites is sufficiently common that there is little need here for thorough documentation." However, in many plutons the textural relationships between biotite and hornblende are ambiguous (e.g., Speer 1987), and magma mixing can disturb and invert textural relationships (Frost and Mahood 1987).

Smelik et al. (1991) presented transmission electron microscope evidence for fine-scale exsolution between hornblende and actinolite in a metagabbro. The altered amphibole consists of lamellae of hornblende and actinolite intergrown on a 5-15 nm scale. The beam size during our microprobe analyses was 1 μm in diameter (with a somewhat larger activation volume), and thus would average over 100 or more lamellae of such dimensions. It is likely that the continuous range in composition from hornblende to actinolite (Fig. 6) reflects varying proportions of hornblende and actinolite lamellae rather than true compositional variation on the unit cell scale.

IMPLICATIONS

The Half Dome Granodiorite is considered a classic igneous rock, and yet some of the minerals in it record extensive recrystallization and reaction at temperatures well below the nominal solidus (~650 °C). The hornblende phenocrysts discussed above, in spite of their large size, euhedral form, and fresh appearance, have undergone extensive closed-system reaction to a set of greenschist-facies minerals, leaving behind only remnants of the original hornblende. The phenocrysts are in effect reaction cells that retained the outward appearance of hornblende in spite of the complexity within. Other minerals are consistent with this; K-feldspar has recrystallized down to temperatures on the order of 400 °C or lower (Johnson and Glazner 2010), magnetite has exsolved essentially all of its ulvöspinel component (Glazner, unpublished data), and thin films of albite coat most plagioclase-K-feldspar contacts, giving 3-feldspar assemblages that span the peristerite gap (Glazner and Johnson 2013).

The rock is mineralogically in the greenschist facies and yet is undeniably an igneous rock. We propose that this is a natural consequence of incremental emplacement, because slow cooling under oscillating temperature conditions promotes exsolution and mineral reequilibration. Classic plutonic textures, such as that of the Half Dome Granodiorite, reflect the metamorphic part of their cooling history as well as the supersolidus igneous part.

Acknowledgments

This work was undertaken as an undergraduate honors thesis at the University of North Carolina with the support of the Department of Geological Sciences. Reviewers Martin Streck and Mike Dungan and Associate Editor Fidel Costa provided excellent, constructive reviews that greatly improved the clarity of our work. We would like to thank Audrey Horne for her assistance with SEM operation while completing her own honors thesis, Nick Foster for assistance with microprobe analyses, and Eugene Smelik for his comments on amphiboles. This research was supported by the Walter H. Wheeler Fund, NSF grant EAR-1250505 and the Mary Lily Kenan Flagler Bingham trust.

References cited

Abbott, R.N., Jr. (1981) AFM liquidus projections for granitic magmas, with special reference to hornblende, biotite and garnet. The Canadian Mineralogist, 19, 103-110.

Ague, J.J., and Brimhall, G. H. (1988) Magmatic arc asymmetry and distribution of anomalous plutonic belts in the batholiths of California; effects of assimilation, crustal thickness, and depth of crystallization. Geological Society of America Bulletin, 100, 912-927.

Anderson, J.L., Barth, A.P, Wooden, J.L. and Mazdab, F. (2008) Thermometers and thermobarometers in granitic systems. Reviews in Mineralogy & Geochemistry, 69, 121-142.

Anderson, J.L., and Smith, D.R. (1995) The effects of temperature and f_{O2} on the Al-in-hornblende barometer. American Mineralogist, 80, 549-559.

Bachmann, O., and Dungan, M.A. (2002) Temperature-induced Al-zoning in hornblendes of the Fish Canyon magma, Colorado. American Mineralogist, 87, 1062-1076.

Bachmann, O., Dungan, M.A., and Bussy, F. (2005) Insights into shallow magmatic processes in large silicic magma bodies; the trace element record in the Fish Canyon magma body, Colorado. Contributions to Mineralogy and Petrology, 149, 338-349.

Bateman, P.C. (1961) Granitic formations in the east-central Sierra Nevada near Bishop, California. Geological Society of America Bulletin, 72, 1521-1537.

Bateman, P.C. (1992) Plutonism in the central part of the Sierra Nevada batholith, California. U.S. Geological Survey Professional Paper, 1483, 186.

Bateman, P.C., and Chappell, B.W. (1979) Crystallization, fractionation, and solidification of the Tuolumne Intrusive Series, Yosemite National Park, California. Geological Society of America Bulletin, 90, 465-482.

Boehnke, P., Watson, E.B., Trail, D., Harrison, T.M., and Schmitt, A.K. (2013) Zircon saturation re-revisited. Chemical Geology, 351, 324-334.

Booth, B. (1968) Petrogenetic significance of alkali feldspar megacrysts and their inclusions in Cornubian granites. Nature, 217(5133), 1036-1038.

Bowen, N.L., 1928, The Evolution of the Igneous Rocks, Princeton, New Jersey, Princeton University Press, 333 p.

Coleman, D.S., Gray, W., and Glazner, A.F. (2004) Rethinking the emplacement and evolution of zoned plutons: geochronologic evidence for incremental assembly of the Tuolumne Intrusive Suite, California. Geology, 32, 433-436.

Coleman, D. S., Bartley, J. M., Glazner, A. F., and Law, R. D. (2005) Incremental Assembly and Emplacement of Mesozoic Plutons in the Sierra Nevada and White and Inyo Ranges, California. Geological Society of America Field Forum Field Trip Guide (Rethinking the Assembly and Evolution of Plutons: Field Tests and Perspectives, 7–14 October 2005), 59 p.

Crosby, W.O. (1900) On the origin of phenocrysts and the development of the porphyritic texture in igneous rocks: American Geologist, 299-300.

Davis, J.W., Coleman, D.S., Gracely, J.T., Gaschnig, R., and Stearns, M. (2012) Magma accumulation rates and thermal histories of plutons of the Sierra Nevada Batholith, CA. Contributions to Mineralogy and Petrology, 163, 449-465.

Devine, J.D., Rutherford, M.J., and Gardner, J.E. (1998) Petrologic determination of ascent rates for the 1995-1997 Soufriere Hills Volcano andesitic magma. Geophysical Research Letters, 25, 3673-3676.

Dodge, F.C.W., Papike, J.J., and Mays, R.E. (1968) Hornblendes from granitic rocks of the central Sierra Nevada Batholith, California. Journal of Petrology, 9, 378-410.

Frost, T.P., and Mahood, G.A. (1987) Field, chemical, and physical constraints on mafic-felsic magma interaction in the Lamarck Granodiorite, Sierra Nevada, California. Geological Society of America Bulletin, 99, 272-291.

Gibbons, W., and Horak, J. (1984) Alpine metamorphism of Hercynian hornblende granodiorite beneath the blueschist facies *schistes lustrés* nappe of NE Corsica. Journal of Metamorphic Geology, 2, 95-113.

Gilbert, G.K. (1906) Gravitational assemblage in granite. Geological Society of America Bulletin, 17, 321-328.

Glazner, A.F., Coleman, D.S., and Bartley, J.M. (2008) The tenuous connection between high-silica rhyolites and granodiorite plutons. Geology, 36, 183-186.

Glazner, A.F., and Johnson, B.R. (2013) Late crystallization of K-feldspar and the paradox of megacrystic granites. Contributions to Mineralogy and Petrology, 166, 777-799.

Grapes, R. (1975) Actinolite-hornblende pairs in metamorphosed gabbros, Hidaka Mountains, Hokkaido. Contributions to Mineralogy and Petrology, 49, 125-140.

Gray, W., Glazner, A.F., Coleman, D.S., and Bartley, J.M. (2008) Long-term geochemical variability of the Late Cretaceous Tuolumne Intrusive Suite, central Sierra Nevada, California. Geological Society, London, Special Publications, 304, 183-201.

Hammarstrom, J.M., and Zen, E. (1986) Aluminum in hornblende; an empirical igneous geobarometer. American Mineralogist, 71, 1297-1313.

Harker, A., Marr, J.E. (1891) The Shap Granite, and the associated igneous and metamorphic rocks. Quarterly Journal of the Geological Society, 47, 266-328.

Holtz, F., and Johannes, W. (1994) Maximum and minimum water contents of granitic melts; implications for chemical and physical properties of ascending magmas. Lithos, 32, 149-159.

Humphreys, M.C.S., Blundy, J.D., and Sparks, R.S.J. (2006) Magma evolution and open-system processes at Shiveluch Volcano; insights from phenocryst zoning. Journal of Petrology, 47, 2303-2334.

Humphreys, M.C.S., Edmonds, M., Christopher, T., and Hards, V. (2009) Chlorine variations in the magma of Soufrière Hills Volcano, Montserrat: Insights from Cl in hornblende and melt inclusions. Geochimica et Cosmochimica Acta, 73, 5693-5708.

Johnson, B.R., and Glazner, A.F. (2010) Formation of K-feldspar megacrysts in granodioritic plutons by thermal cycling and late-stage textural coarsening. Contributions to Mineralogy and Petrology, 159, 599-619.

Johnson, M.C., and Rutherford, M.J. (1989) Experimentally determined conditions in the Fish Canyon Tuff, Colorado, magma chamber. Journal of Petrology, 30(3), 711-737.

Kelley, V.C., and Branson, O.T. (1947) Shallow, high-temperature pegmatites, Grant County, New Mexico. Economic Geology, 42, 699-712.

Klein, C. (1969) Two-amphibole assemblages in the system actinolite-hornblende-glaucophane. American Mineralogist, 54, 212-237.

Leake, B.E., Woolley, A.R., Arps, C.E.S., Birch, W.D., Gilbert, M.C., Grice, J.D., Guo, Y. (1997) Nomenclature of amphiboles; report of the subcommittee on amphiboles of the international mineralogical association, commission on new minerals and mineral names. American Mineralogist, 82, 1019-1037.

Lofgren, G. (1980) Experimental studies on the dynamic crystallization of silicate melts. In R.B. Hargraves, Ed. Physics of Magmatic Processes, p. 487-551. Princeton University Press, Princeton, N.J.

Naney, M.T., and Swanson, S.E. (1980) The effect of Fe and Mg on crystallization in granitic systems. American Mineralogist, 65, 638-653.

Okamoto, A., and Toriumi, M. (2005) Progress of actinolite-forming reactions in mafic schists during retrograde metamorphism: an example from the Sanbagawa metamorphic belt in central Shikoku, Japan. Journal of Metamorphic Geology, 23, 335-356.

Piwinskii, A.J. (1968) Experimental studies of igneous rock series, central Sierra Nevada batholith, California. Journal of Geology, 76, 548-570.

Putnam, R., Glazner, A.F., Coleman, D.S., Kylander-Clark, A.R.C., Pavelsky, T., and Abbot, M.I. (2015) Plutonism in three dimensions: Field and geochemical relations on the southeast face of El Capitan, Yosemite National Park, California. Geosphere, 11, GES01133-1.

Rutherford, M.J., and Devine, J.D. (2003) Magmatic conditions and magma ascent as indicated by hornblende phase equilibria and reactions in the 1995-2002 Soufriere Hills magma. Journal of Petrology, 44, 1433-1454.

Sato, H. (2004) Experimental petrology of the 1991-1995 Unzen dacite, Japan. Part II: Cl/OH partitioning between hornblende and melt and its implications for the origin of oscillatory zoning of hornblende phenocrysts. Journal of Petrology, 46, 339-354.

Smelik, E.A., Nyman, M.W., Veblen, D.R. (1991) Pervasive exsolution within the calcic amphibole series: TEM evidence for a miscibility gap between actinolite and hornblende in natural samples. American Mineralogist, 76, 1184-1204.

Speer, J.A. (1987) Evolution of magmatic AFM mineral assemblages in granitoid rocks: The hornblende + melt = biotite reaction in the Liberty Hill pluton, South Carolina. American Mineralogist, 72, 863-878.

Straub, S.M., and Martin-Del Pozzo, A.L. (2001) The significance of phenocryst diversity in tephra from recent eruptions at Popocatepetl volcano (central Mexico). Contributions to Mineralogy and Petrology, 140, 487-510.

Vernon, R.H. (1986) K-feldspar megacrysts in granites; phenocrysts, not porphyroblasts. Earth-Science Reviews, 23, 1-63.

Watson, E.B., and Harrison, T.M. (1983) Zircon saturation revisited; temperature and composition effects in a variety of crustal magma types. Earth and Planetary Science Letters, 64, 295-304.

FIGURE CAPTIONS

Figure 1. Geologic map of the Tuolumne Intrusive Suite in Yosemite National Park, California, adapted from Bateman (1992). Star marks the sampling location at Tenaya Lake where phenocrysts were collected.

Figure 2. Half Dome hornblende phenocrysts, despite their euhedral form and unaltered appearance, show abundant mineral inclusions and extreme compositional zoning. (**a**) Loose hornblende phenocrysts are readily collected from the grus. (**b**) False-color backscatter image of crystal 3 cut through the center perpendicular to c. (**c**) Mineral map of a subarea of crystal 3

produced by supervised classification of X-ray maps (see Supplementary Figure 1). Inclusions make up 53 area % of this crystal and include every phase in the granodiorite as well as greenschist facies metamorphic minerals.

Figure 3. Proportions of mineral inclusions in five hornblende crystals cut through their centers. Mineral areas were calculated from supervised classification of X-ray maps (see Supplementary Figure 1). All but number 6 were cut perpendicular to *c*; 6 was cut perpendicular to *a*. “Other” includes magnetite, apatite, zircon, epidote, muscovite and quartz.

Figure 4. A composite BSE image of a traditionally prepared polished section of Half Dome Granodiorite hosting a prominent hornblende phenocryst. Mineral composition has been approximated from BSE brightness. Though the hornblende crystal section has not been oriented relative to its crystal axes, abundant inclusions and prominent aconcentric elemental zoning are evident. Hbl = amphiboles from hornblende to actinolite, Ab = albite, Kspr = K-feldspar, Mag = magnetite, Chl = chlorite, Bt = biotite.

Figure 5. BSE image of crystal #5 showing approximately 36 area % inclusions and locations of electron microprobe analyses. Mineral labels as in Figure 4. Red and white circles mark the locations of electron microprobe analyses.

Figure 6. Large internal compositional variations observed in Half Dome Granodiorite hornblende phenocrysts. (**left**) Wt% Al plotted against wt% Mg, with approximate mineral names derived from Leake et al (1997). The phenocrysts include areas of actinolite, ferroactinolite and ferrohornblende. (**right**) Wt% Al by distance from the center of the crystals. Different marker types indicate measurements from different crystals. The red-rimmed white circles indicate measurements from the traverse marked in Figure 5. Variations in Al are large and show no concentric pattern.

Figure 7. Elemental variations within Half Dome hornblende phenocrysts show a diverse array of zoning styles which are difficult to explain within current models of phenocryst formation. (**a**) Zones have rounded but distinct edges, and an overall pattern suggestive of brecciation. (**b**) Complex angular zoning combining blurred and sharp-edged zones. (**c**) Sharp-edged angular zones with lesser internal variations. (**d**) Large angular zones with soft-edged internal zoning.

Figure 8. Whole crystal compositions plot between the high-Al amphibole (magnesiohornblende composition) and biotite spot analyses. These results suggest that the phenocrysts were initially magnesiohornblende with inclusions of biotite and possibly magnetite, and that the other including minerals formed as hornblende was converted to actinolite under greenschist conditions without any compositional modification by fluids.

Figure 9. Thermobarometric estimates for the Half Dome Granodiorite using various methods. Blue curve is the solution of Anderson and Smith (1995) for hornblende with 7 wt% Al_2O_3 (Fig. 8); red circles are from hornblende-plagioclase thermobarometry (Gray et al. 2008); and blue squares are estimates derived from aplite dikes and zircon saturation using the method of Putnam et al. (2015). At a given temperature the 7 wt% hornblende curve yields a higher *P* than the hornblende-plagioclase and aplite-zircon estimates, but all indicate crystallization at low *P* (<200 MPa; see text for discussion). Water-saturated granite solidus from Holtz and Johannes (1994).

Figure 1

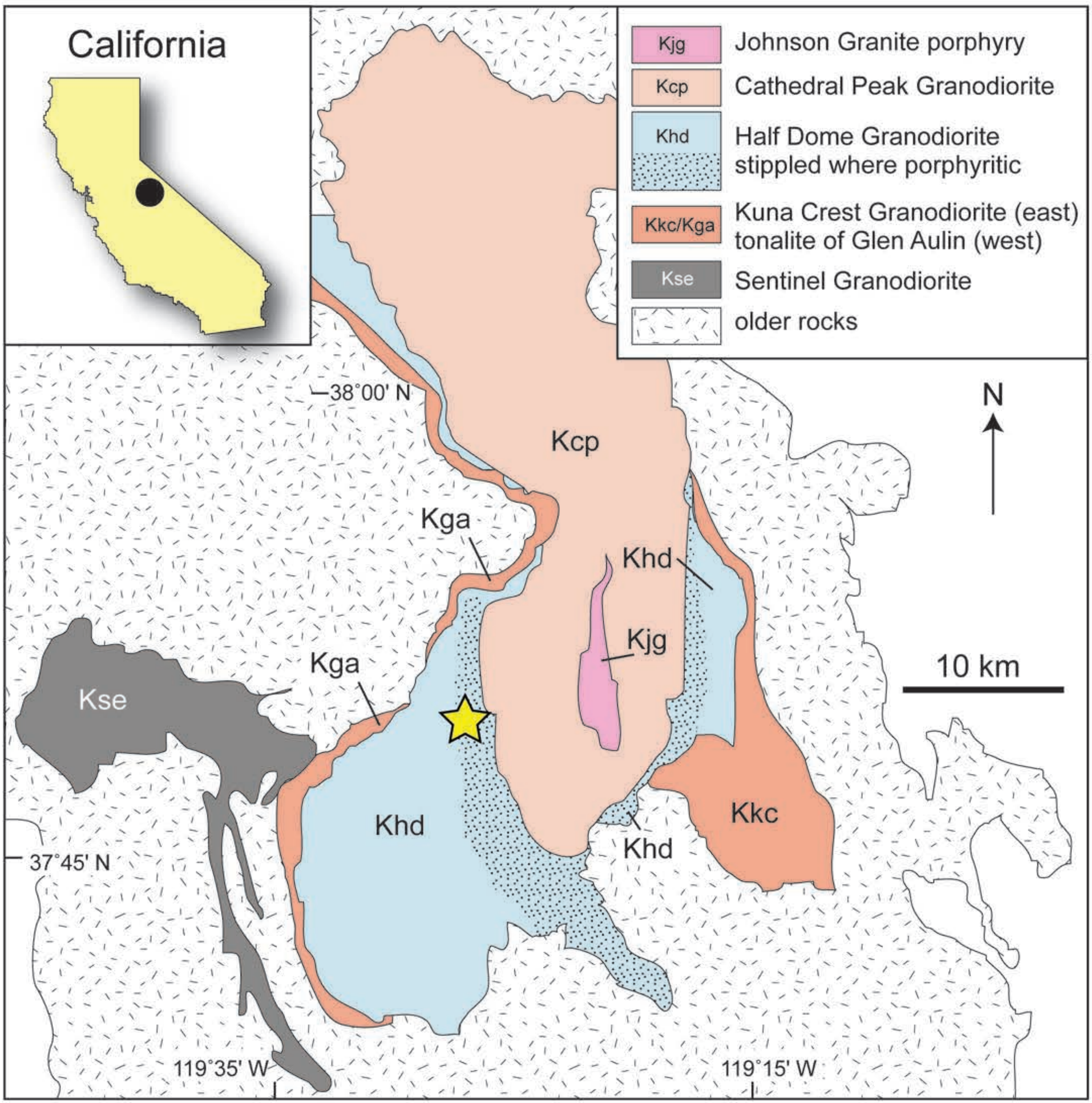

California
Kjg
Johnson Granite porphyry
Kcp
Cathedral Peak Granodiorite
Khd
Half Dome Granodiorite
stippled where porphyritic
Kkc/Kga
Kuna Crest Granodiorite (east)
tonalite of Glen Aulin (west)
Kse
Sentinel Granodiorite
older rocks
38°00' N
N
Kcp
Kga
Khd
Kjg
10 km
Kga
Kse
Khd
Kkc
Khd
37°45' N
119°35' W
119°15' W

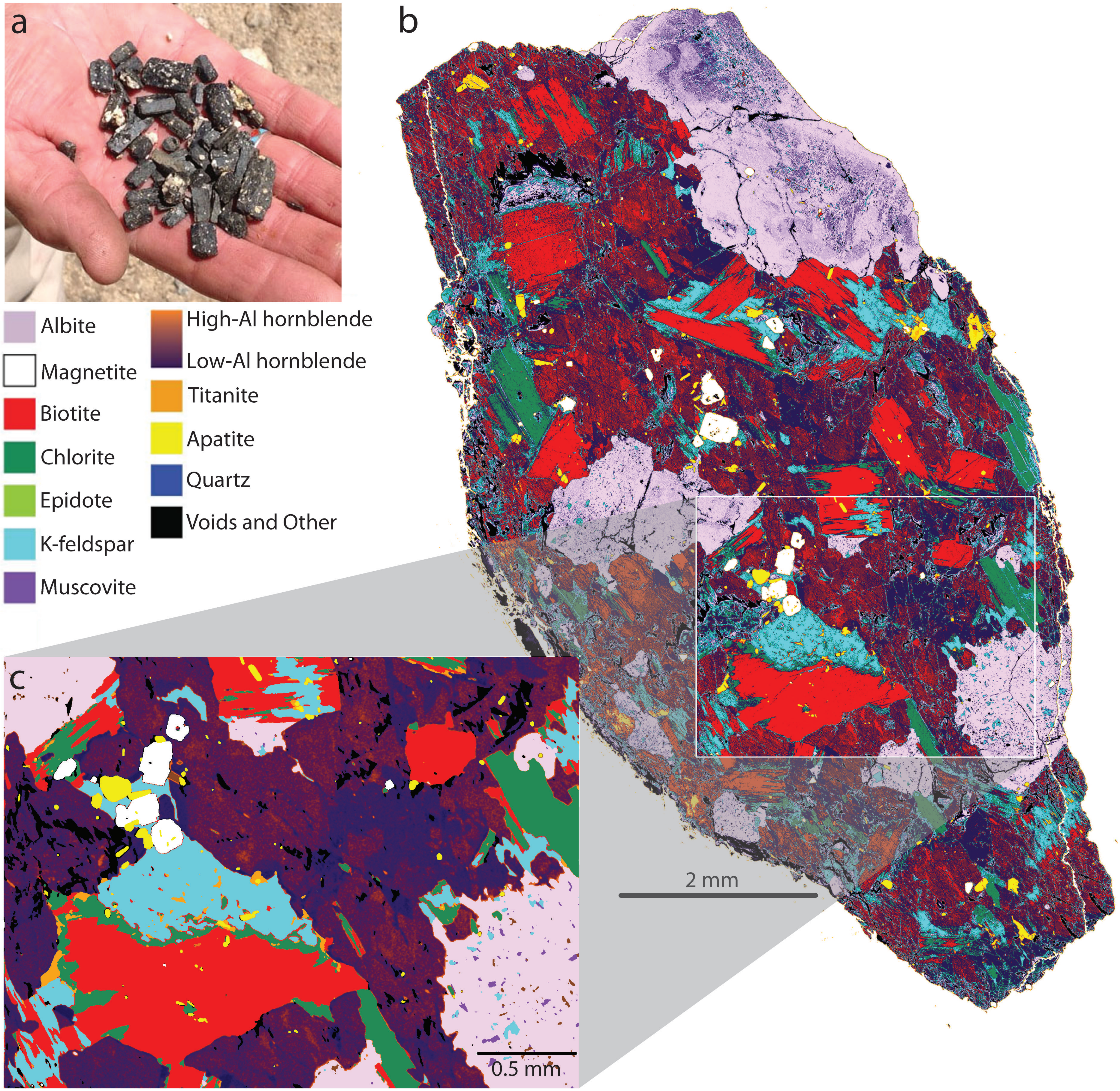
a
b
c
Albite
Magnetite
Biotite
Chlorite
Epidote
K-feldspar
Muscovite
High-Al hornblende
Low-Al hornblende
Titanite
Apatite
Quartz
Voids and Other
2 mm
0.5 mm

Figure 2

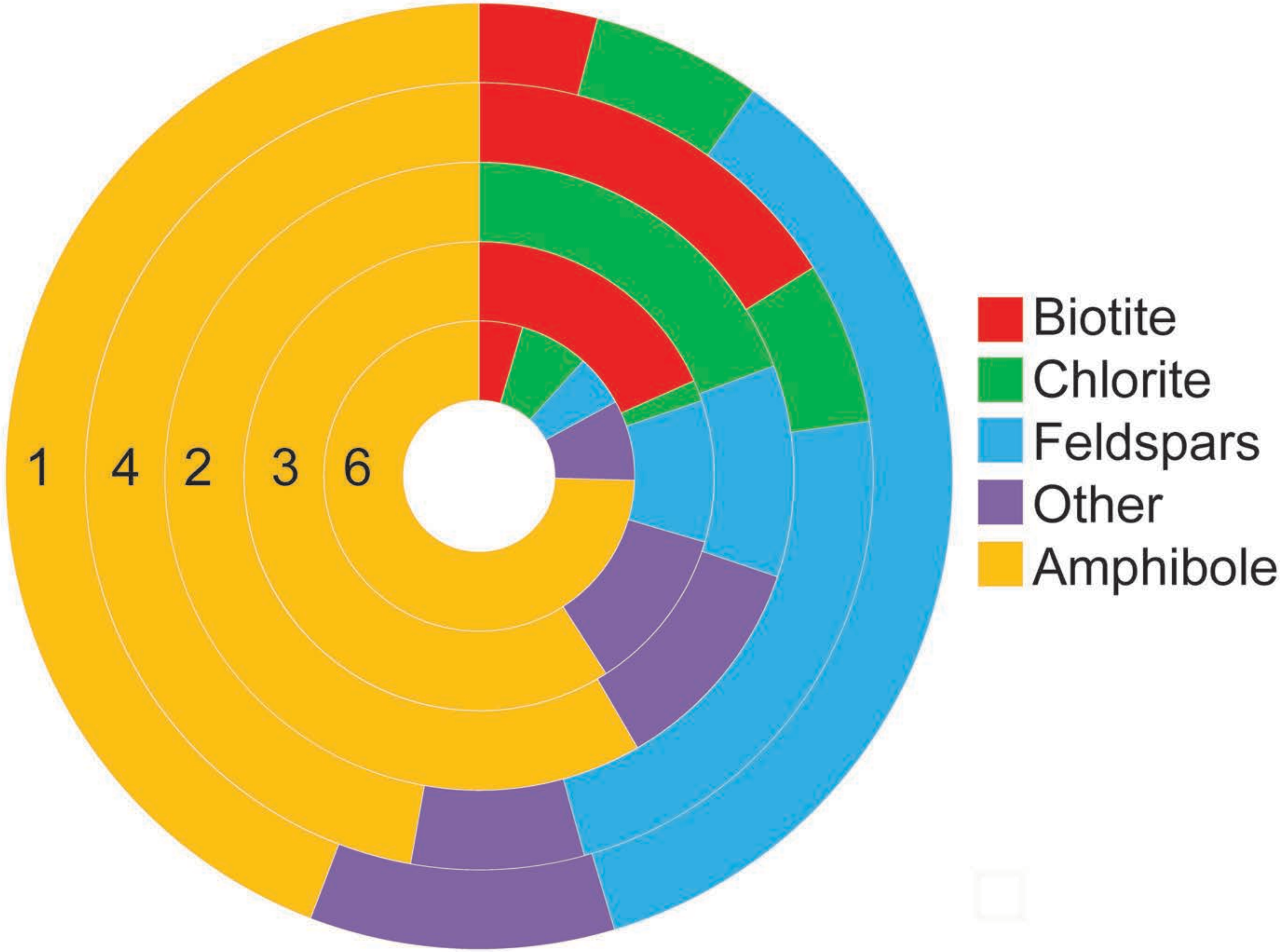

Figure 3

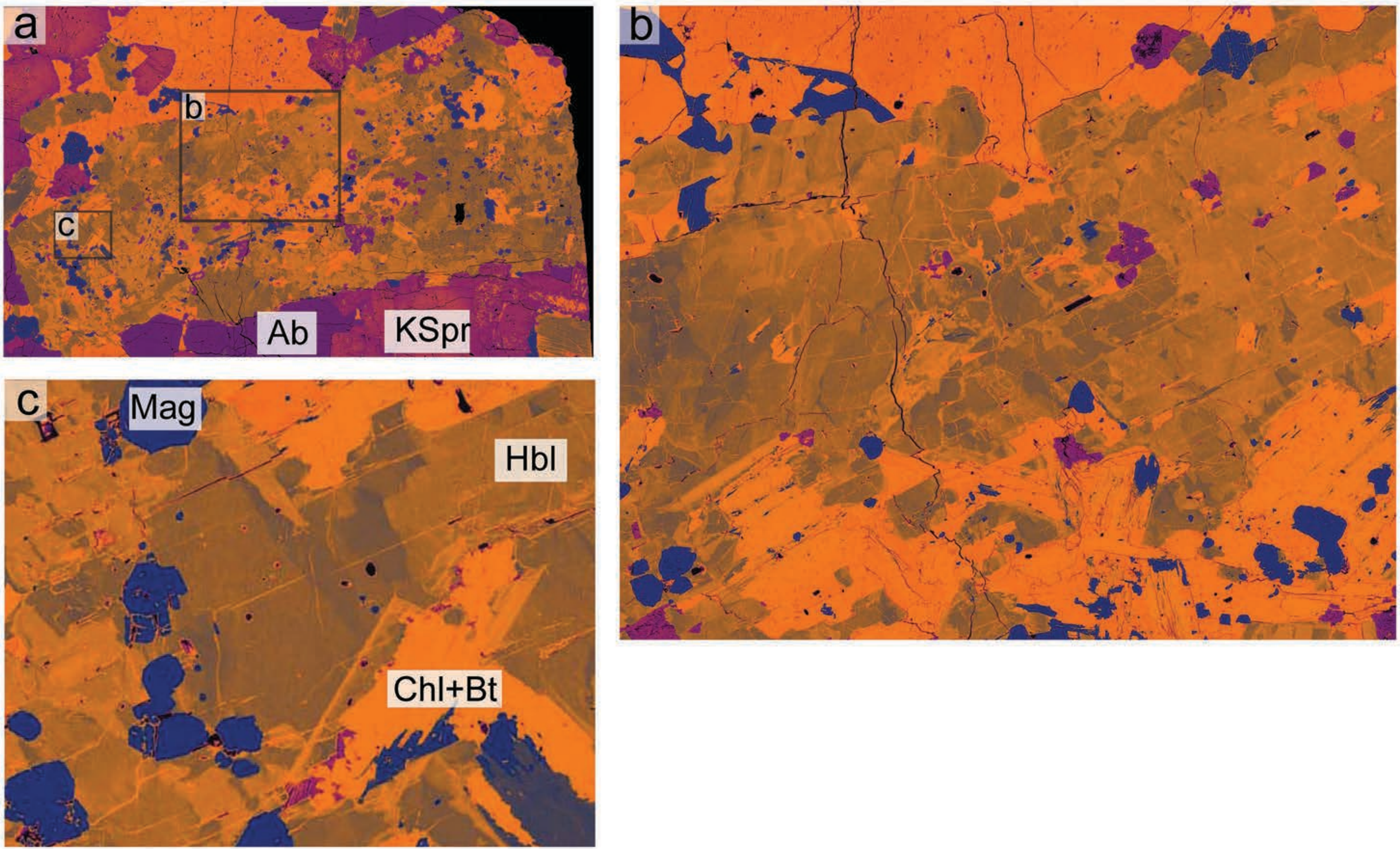

Figure 4

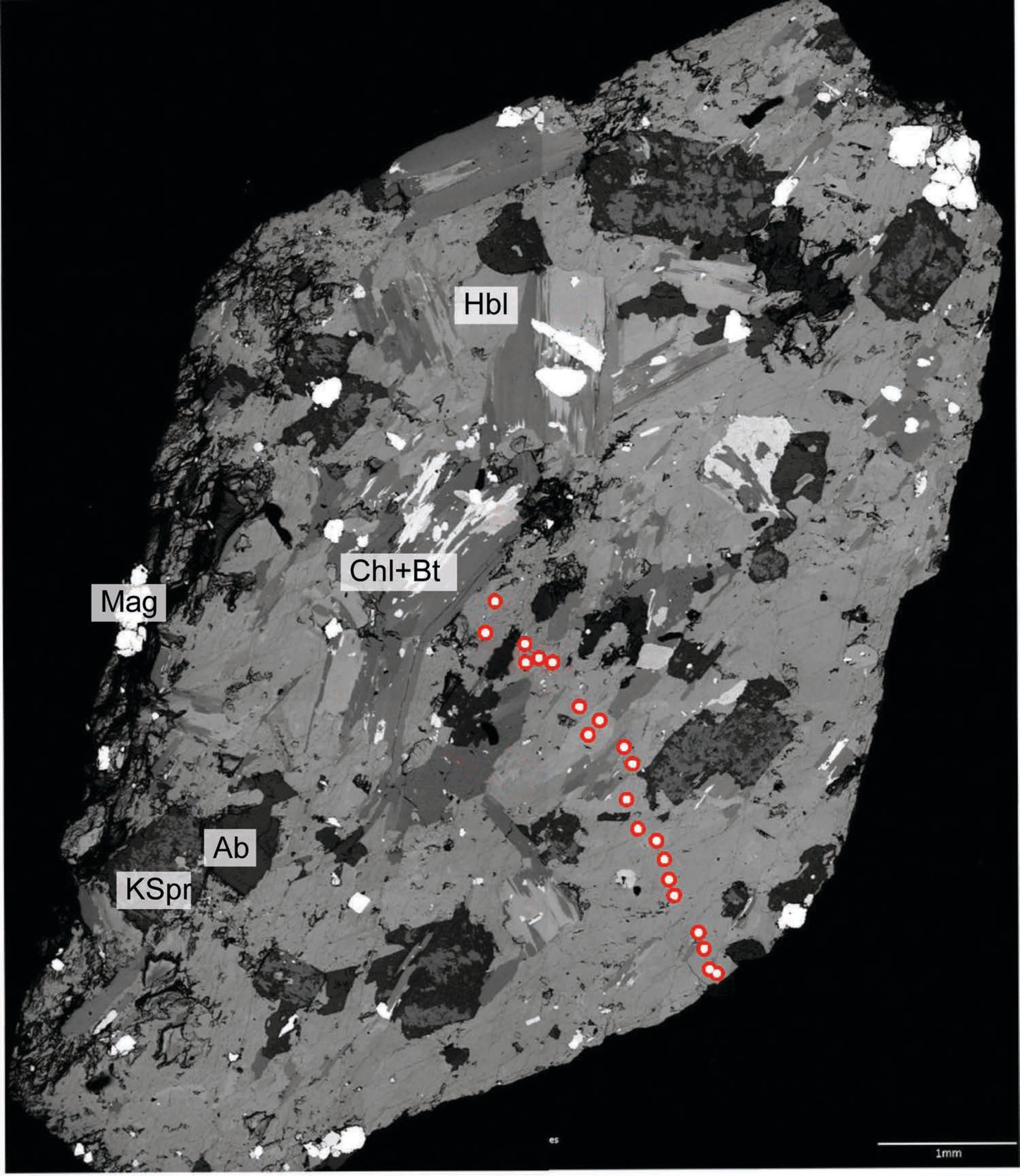

Figure 5

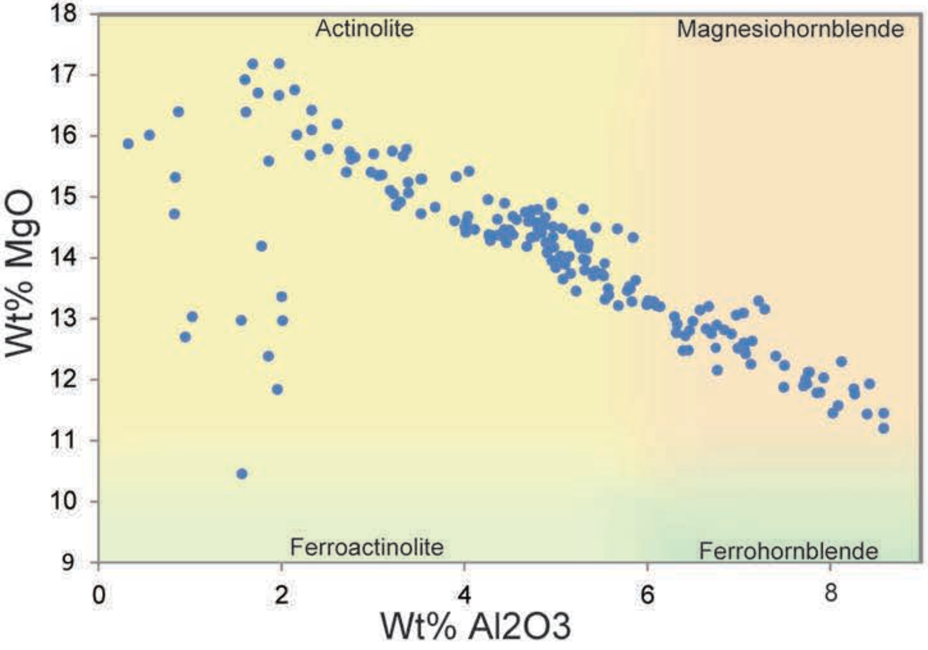
Actinolite
Magnesiohornblende
Ferroactinolite
Ferrohornblende
Wt% MgO
Wt% Al2O3
18
17
16
15
14
13
12
11
10
9
0
2
4
6
8

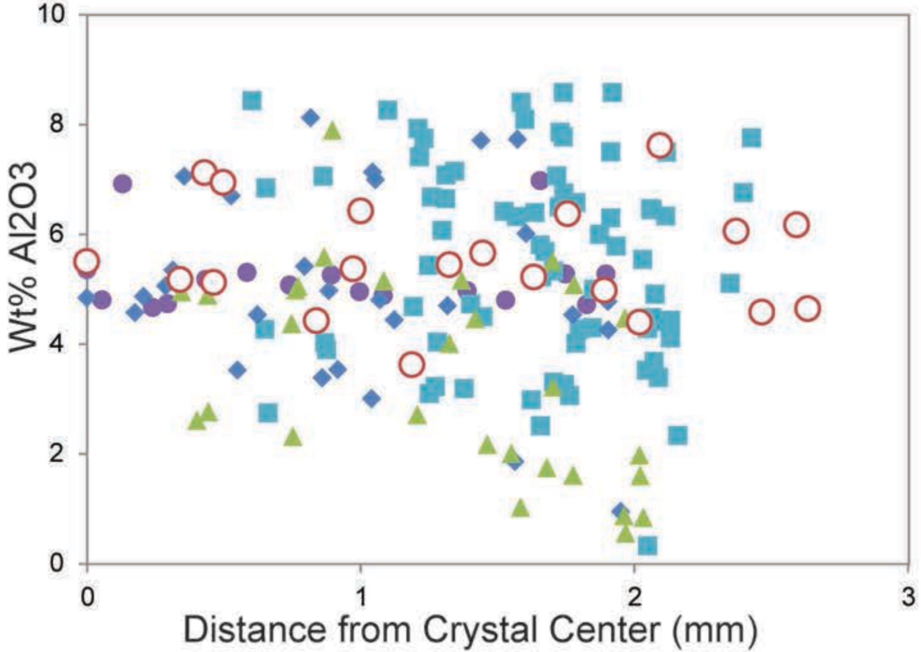
Wt% Al2O3
Distance from Crystal Center (mm)
10
8
6
4
2
0
1
2
3

Figure 6

Table 1. Summary of chemical analyses and Structural Formulae

	Avg Biotite[a]	Avg Whole Xtal	Representative Amphibole Spot Analyses				
			Hbl 3 P28	Hbl 5 P21	Hbl 3 P7	Hbl 2-P6	Hbl 5 P10
SiO_2 (wt%)	37.71	46	52.23	52.07	51.33	45.88	43.84
TiO_2 (wt%)	2.69	1.42	0.00	0.13	0.33	1.01	1.19
Al_2O_3 (wt%)	14.68	8.21	1.79	2.51	4.06	7.06	8.59
FeO (wt%)	18.41	16.21	14.42	11.26	12.11	14.83	15.31
MgO (wt%)	12.89	12.63	14.19	15.78	15.41	12.60	11.2
MnO(wt%)	0.66	0.65	0.56	0.87	0.79	0.65	0.72
CaO (wt%)	0.01	9.86	11.89	11.90	11.80	11.63	11.24
Na_2O (wt%)	0.07	1.04	0.57	0.32	0.69	1.06	1.23
K_2O (wt%)	8.79	1.7	0.10	0.16	0.26	0.70	0.78
Total Ox.	95.91	97.72	95.75	95.00	96.78	95.42	94.10
Si(T)	2.84	*	7.73	7.67	7.44	6.88	6.72
Al(T)	1.30	*	0.27	0.33	0.56	1.12	1.28
Σ(T)	4.14	*	8.00	8.00	8.00	8.00	8.00
Al(M1,2,3)	0.72	*	0.04	0.10	0.14	0.13	0.27
Ti(M1,2,3)	0.15	*	0.00	0.01	0.04	0.11	0.14
Fe^{3+}(M1,2,3)	0.00	*	0.23	0.17	0.30	0.56	0.49
Mg(M1,2,3)	1.45	*	3.13	3.46	3.33	2.82	2.56
Mn(M1,2,3)	0.04	*	0.07	0.11	0.10	0.08	0.09
Fe^{2+}(M1,2,3)	1.16	*	1.53	1.14	1.10	1.29	1.45
Ca(M1,2,3)	0.00	*	0.00	0.00	0.00	0.00	0.00
Σ(M1,2,3)	5.00	*	5.00	5.00	5.00	5.00	5.00
Fe(M4)	1.61	*	0.03	0.08	0.07	0.01	0.02
Ca(M4)	0.00	*	1.89	1.88	1.83	1.87	1.85
Na(M4)	0.39	*	0.09	0.05	0.10	0.12	0.14
Σ(M4)	2.00	*	2.00	2.00	2.00	2.00	2.00
Ca(A)	0.00	*	0.00	0.00	0.00	0.00	0.00
Na(A)	0.01	*	0.07	0.05	0.10	0.19	0.23
K(A)	0.84	*	0.02	0.03	0.05	0.13	0.15
Σ(A)	0.85	*	0.09	0.08	0.15	0.32	0.38
OH	2.00	*	2.00	2.00	2.00	2.00	2.00
Σ(Cat.)	12.00	*	15.09	15.08	15.15	15.32	15.38

[a] A single anomalously phlogopitic spot analysis was excluded from the average biotite calculation; see Supplementary Tables 1 and 2 for all spot analyses.

Average biotite formula calculated assuming 2 OH and all ferrous iron.

Amphibole formulae calculated following the methods of Anderson and Smith (1995).

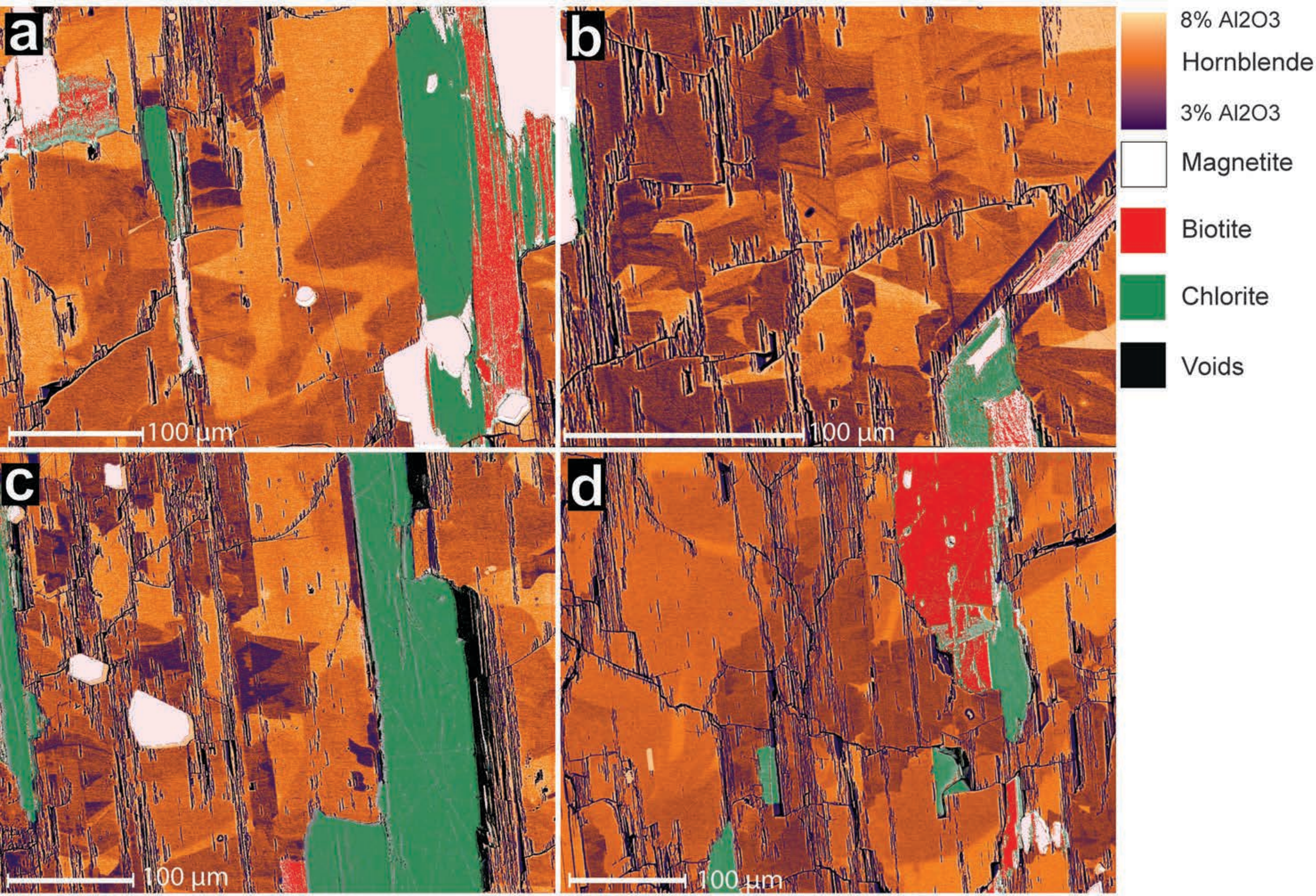
a
b
c
d
100 µm
100 µm
100 µm
100 µm
8% Al2O3
Hornblende
3% Al2O3
Magnetite
Biotite
Chlorite
Voids

Figure 7

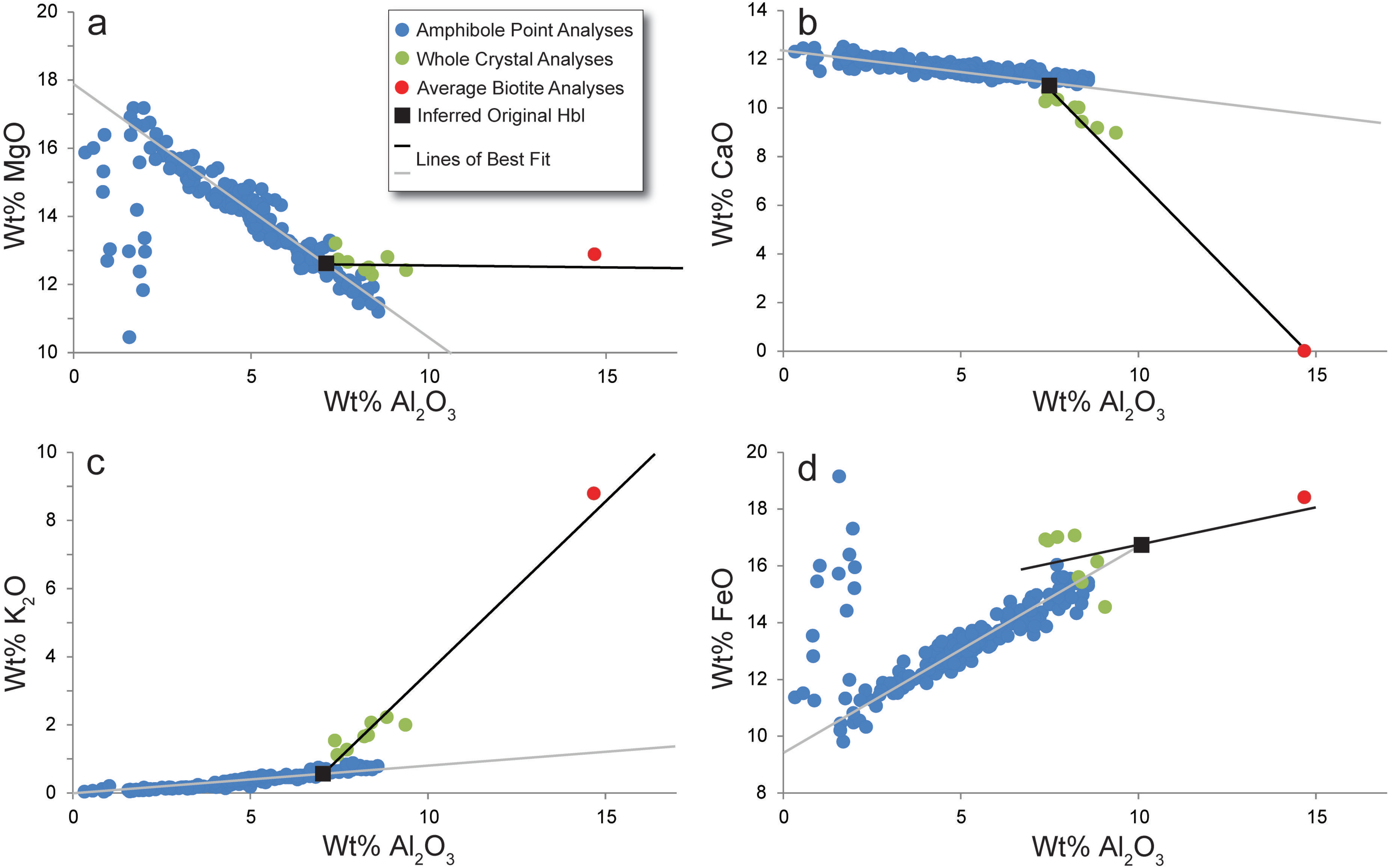
a
b
c
d
Amphibole Point Analyses
Whole Crystal Analyses
Average Biotite Analyses
Inferred Original Hbl
Lines of Best Fit
Wt% MgO
Wt% CaO
Wt% K_2O
Wt% FeO
Wt% Al_2O_3
Wt% Al_2O_3
Wt% Al_2O_3
Wt% Al_2O_3

Figure 8

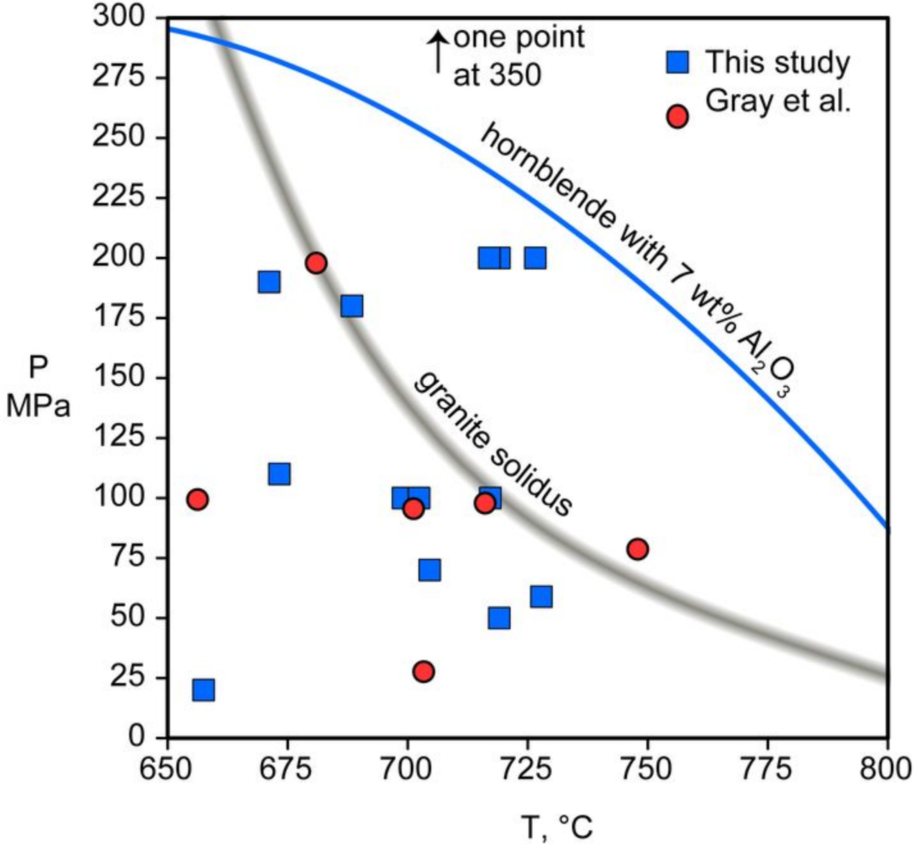

one point at 350
This study
Gray et al.
hornblende with 7 wt% Al_2O_3
granite solidus
P MPa
T, °C
300
275
250
225
200
175
150
125
100
75
50
25
0
650
675
700
725
750
775
800

Figure 9